Optimization of a New Scintillation Gas Detector Used to Localize Electrons Emitted by ^{99m}Tc

Nicole Barthe, Philippe Coulon, Claude Hennion, Dominique Ducassou, Bernard Basse-Cathalinat and Georges Charpak

Laboratoire de Biophysique, Université Victor Segalen Bordeaux 2, Bordeaux; Ecole Supérieure de Physique et Chimie Industrielles, Paris, France

We have developed a scintillation gas detector to localize electrons emitted by ^{99m}Tc. This type of detector allows direct quantification of images and so provides a clear advantage over autoradiographic film. We have optimized the device to give an image spatial resolution that closely approximates that of typical autoradiographic film. To improve this resolution, it was necessary to select only low-energy electrons (2 and 15 keV) and to devise novel detection and localization techniques for the ionizing particles. **Methods:** A parallel-plate proportional avalanche chamber is subject to a uniform electrical field and amplifies the number of released electrons through collisions of ionizing particles in the gas mixture. Light emitted by the gas scintillator during the avalanche process is collected by a highly intensified charge coupled device camera. The centroid of each resulting light distribution is calculated, resulting in a quantitative mapping of the sample's activity. Insertion of the sample within the gas volume improves the efficiency and so provides a method that is both very sensitive and linear. **Results:** We have shown that in a parallel-plate structure, the application of a high electrical field to the surface of the sample and the selection of appropriate light spots, according to their morphology, can overcome localization errors due to the particles' trajectories. We have obtained a resolution of the order of 30 μm, using electrons from ^{99m}Tc. **Conclusion:** This detection technique allows considerable improvement in image resolution. This "electron camera" is a serious rival to existing autoradiographic techniques, because it provides certain other advantages, including direct quantification, linearity, high dynamic range and low noise levels. Thus, new perspectives are made available in quantitative double tracer autoradiography, because electrons can be selected for imaging as a function of their energy.

Key Words: ^{99m}Tc; autoradiography; scintillation gas detector; avalanche chamber

J Nucl Med 1999; 40:868–875

Technetium-99m is extensively used in nuclear medicine. Most investigations in vivo use this tracer because of its short physical half-life and its emission of 140-keV gamma rays. Therefore, many research groups are actively investigating the radiolabeling of a variety of molecules or cellular components with this radioactive tracer (*1–4*).

The development of these radiolabeled molecules and the necessary pharmacokinetic studies require autoradiographic techniques. These normally use β emitters such as ^{3}H or ^{35}S. However, these autoradiographic techniques, in principle, also can be performed with emitters such as ^{99m}Tc, because this radionuclide emits many low-energy electrons while decaying.

A novel imaging system has been developed to localize electrons emitted by ^{99m}Tc. The detector is a gas chamber, using technology developed in recent years by Charpak et al. (*5–7*) and Peskov et al. (*8*). However, this chamber has been greatly modified for use with electrons emitted by ^{99m}Tc and to provide optimal performance using this radionuclide. Optimization of this detector was especially directed toward spatial resolution of images.

The aim of this study was to describe the detector, its mode of operation and performance in terms of sensitivity, linearity and spatial resolution.

A comparative study with other tracers, such as ^{3}H and ^{14}C is presented. Images obtained in a rabbit, using two common nuclear medicine radiopharmaceuticals, hexamethyl propyleneamine oxime (HMPAO) and dimercaptosuccinic acid (DMSA), allow the performance of this imaging device to be evaluated.

METHODS AND MATERIALS

Aspects of ^{99m}Tc Radiation

The decay scheme of ^{99m}Tc is relatively complicated, as this radionuclide emits gammas, x-rays and monoenergetic electrons (conversion electrons and Auger electrons). Investigation of the electron emission shows that the electrons which are able to escape from a slice of tissue can be classified into three groups, whose energies (Table 1) are close to 2, 15 and 120 keV (*9*). The 2-keV electrons are strongly absorbed in the biologic specimen, in comparison with the 120-keV electrons. On the other hand, the 2-keV electrons have a much greater probability of emission (0.991 compared with 0.0843). Thus, for a thin slice, as shown in Figure 1, the number of low-energy electrons (2 and 15 keV) that escape from the slice is on the order of 10%. The efficient detection and selection of these low-energy electrons are the most important criteria for improving spatial resolution.

The relative ranges in water and various gases, of electrons emitted by the most commonly used radionuclides in this field, are shown in Table 2.

TABLE 1
Average Electron Energies (E_i) in keV and Yields (n_i) per Decay

^{99m}Tc	
E_i	n_i
0.334	1.98
0.0429	0.0193
0.116	0.747
0.226	1.10
1.82	0.991
2.05	0.0868
2.32	0.0137
2.66	0.0012
15.3	0.0126
17.8	0.0047
119	0.0843
122	0.0059
187	0.0136
140	0.0062

Description of Device

A parallel plate proportional avalanche chamber, under the influence of a uniform electrical field, multiplies the electrons released by passage of an ionizing particle through the gas mixture composed of argon and a low percentage of triethylamine. The light emitted by the gas scintillator during the avalanche process is detected by an intensified charge coupled device (CCD) camera. The count and localization by a centroid calculation of each light distribution creates the quantitative cartography of the activity in the sample.

The insertion of the samples inside the gas volume renders this method exceptionally efficient for very low-energy particles, such as ^{3}H β electrons or the 2-keV conversion electrons in ^{99m}Tc. Each particle emerging from the sample creates at least one primary ionization electron, which initiates an avalanche of about 10^4–10^5 electrons after acceleration by the electric field. This process creates about the same quantity of photons, and the scintillation light recorded by the intensified CCD camera allows detection and localization of the particle (Fig. 2). The spatial resolution of the device is determined by that of the gaseous detector itself and that of the optical readout system.

Since the detection region is limited by parallel planes of electrodes, the multiplication of electrons (G) in the gas under the effect of an electric field increases exponentially with the distance x of the electron from the anode plane: $G = \exp(ax)$, where $1/a$ is the mean free path for an electron. Under these conditions, the electrons nearest to the cathode give rise to the largest electron multiplication. The localization of this maximum of light intensity with the camera overcomes much of the localization error that results from the trajectories of the particles in gas. Moreover, the calculation of the centroid of the light distribution of the spot on the CCD allows us to locate the emission point of the β particule with a spatial resolution better than that of the CCD.

A Two-Stage Structure to Improve Detection

The effect described above increases with the electrical field intensity near the sample, but is limited by a maximum number of electrons between the electrodes. To overcome this limitation, we introduced an additional grid between the sample and the anode (Fig. 3). This allows application of a higher field to the surface of the sample, so creating a high electron amplification in the first stage, whereas the electric field in the second stage is lower and therefore more favorable to the creation of light. This two-stage structure, that we call the high amplification mode, offers both a better resolution for the gaseous detector as a result of the high electrical field near the sample and a better resolution of the optical reading system because of larger light emission.

Spot Selection

Every luminous spot resulting from each particle emerging from the surface of the sample in the gas volume of the detector is recorded by the camera. The examination of these spots according to their morphology–size (number of CCD pixels: n), intensity, shape (ellipticity: e)–allows us to separate the particles detected according to their energy. This can be used to separate tracers of different energies and to reject the more energetic particles. The result is impovement in spatial resolution. In the case of ^{99m}Tc, we then can reject 120-keV electrons and create an image of the sample using only 2- and 15-keV electrons.

RESULTS

Noise

The noise from this device is mainly the result of its detection of cosmic rays. The amplification within the parallel plate structure leads to a decrease in electron multiplication by a factor (e) every distance $(1/a)$ away from the cathode. We can then define a skin layer $(d = 1/a)$ at the surface of the sample outside which a primary ionization will have a low effect. We can then consider that the sensitive volume of the detector is approximately limited to the skin layer (<200 μm thick). The cosmic rays detected are virtually limited to those interacting in this skin layer. We have measured a noise lower than 0.1 cpm/cm^2 in the high amplification mode.
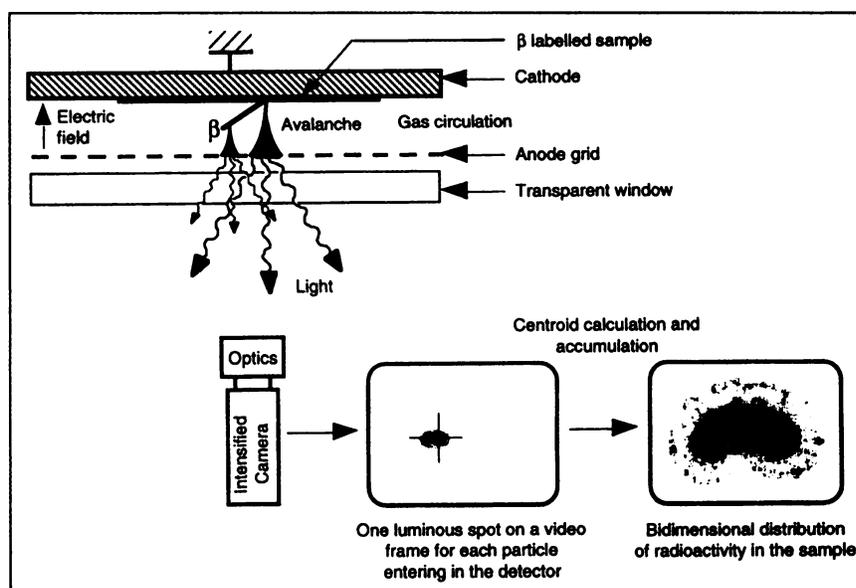
This skin layer also has an advantage of improved
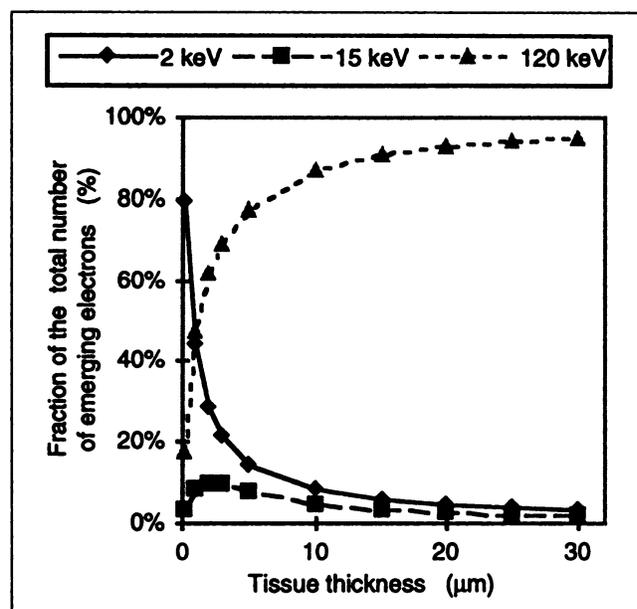
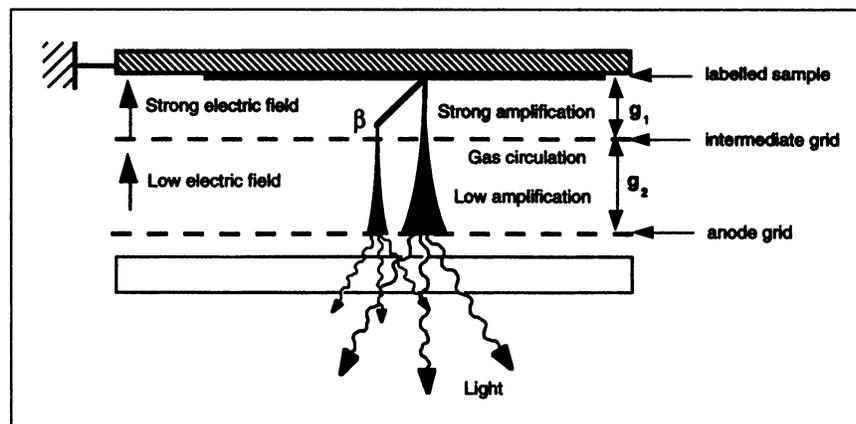**FIGURE 1.** Electrons emerging from biologic tissue sample labeled with ^{99m}Tc.

TABLE 2
Actual Range of Electrons Emitted by Commonly Used Tracers

Tracer		Energy (keV)	Actual Range (mg/cm^2)	(mm) Water (1 g/cm^3)	(mm) Argon 1 bar (1.66 mg/cm^3)	(mm) Xenon 1 bar (5.49 mg/cm^3)
^{32}P	E_{max}	1710	790	7.902	4758	1439
	E_{mean}	695	256	2.568	1546	468
^{33}P	E_{max}	248	65	7.902	391	118
	E_{mean}	76.9	8.61	0.086	52	16
^{14}C	E_{max}	156	28.26	0.283	170	51
	E_{mean}	49	3.97	0.040	24	7
^{3}H	E_{max}	18.6	0.750	0.0075	4.514	1.365
	E_{mean}	5.7	0.098	0.0010	0.590	0.179
^{99m}Tc		2	0.016	0.0002	0.097	0.029
		15	0.518	0.0052	3.118	0.943
		120	18.357	0.1836	110.558	33.437

FIGURE 2. General principle of detection.
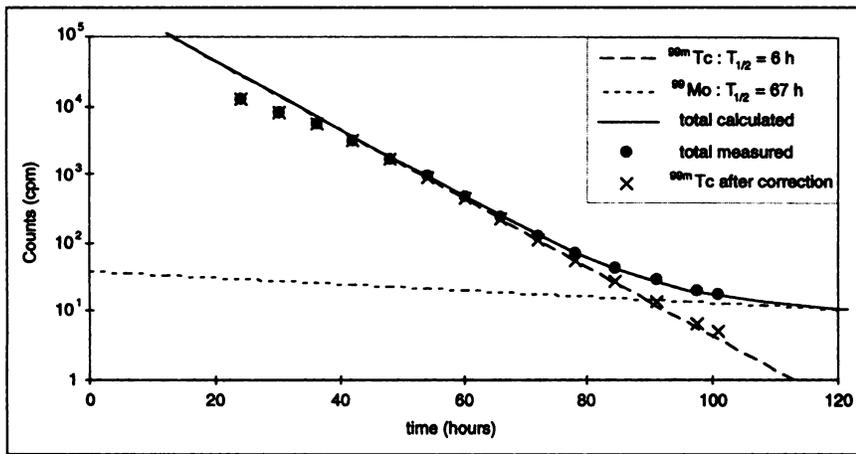

FIGURE 3. High amplification mode in two-stage structure.

FIGURE 4. Linearity measurements using short half-life of ^{99m}Tc.

resolution in the case of ^{99m}Tc labeling, because the detector has a very low sensitivity to long-range gamma rays.

Linearity

To check the linearity of the detector, we used the 6.02 h short half-life of ^{99m}Tc (Fig. 4). Measurement of the counting rate every 6.02 h shows a saturation of more than 2000 cpm, mainly as a result of computer calculation limits that should soon be increased. We also observed an unexpected overcounting after about 10 half-lives. Emissions from the mother of ^{99m}Tc provide the explanation: ^{99}Mo emits electrons of energies 1.23 MeV and 0.45 MeV with a half-life of 67 h. A rapid calculation of the linearity deviation of the measures gives 0.06% of ^{99}Mo traces in the ^{99m}Tc solution at the time when the sample was taken. The correction of the activities for the calculated traces of ^{99}Mo activity shows a good linearity of ^{99m}Tc detection at low activities (with less than 5% deviation).

We also measured the linearity of the detector with a tritium-labeled sample composed of 14 blood deposits with activities increasing incrementally by a factor of 2 and measured with a liquid scintillation detector. Figure 5 illustrates the excellent linearity of the system over about four decades.

Spatial Resolution

Special Sample for Resolution Measurements. To obtain quantitative measurement of the resolution, we designed a special sample consisting of labeled biologic gelatin placed in engraved lines on a microscope slide (Fig. 6). The separation power and resolution of the detector could then be measured by the full width at half maximum of a labeled line (Figs. 7 and 8).

The direct light detection from ultraviolet scintillation of the gas, using a wide diameter ultraviolet transmitting lens (40 mm f/2) and a small optical demagnification factor (reduction by a factor of 5 leading to a readout surface of 24 X 32 mm^2), gave resolutions of the order of 80 and 50 μm, with raw data recorded using ^{3}H and ^{99m}Tc, respectively. By selecting the luminous spots according to their morphology, these resolutions were improved to 50 and 30 μm, respectively. Meanwhile, under the same detection conditions, these resolutions were of the order of 130 and 110 μm for ^{32}P and ^{14}C, respectively (Table 3).

In the case of the tritium-labeled sample, the improvement was the result of rejection of the most energetic part of the β energy spectrum. In the case of ^{99m}Tc, it was the result of rejection of 120-keV conversion electrons. Resolution

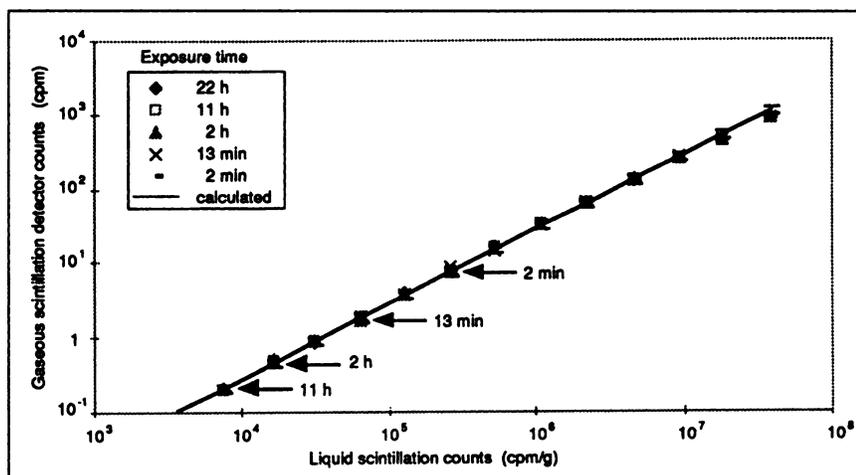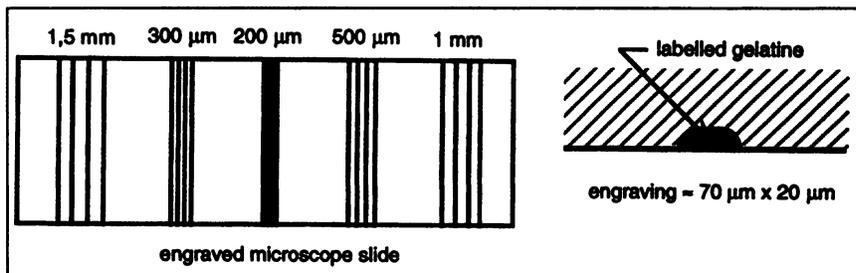**FIGURE 5.** Linearity measurements with ^{3}H; limit of sensitivity after indicated exposure time.

FIGURE 6. Special sample for resolution measurements.

was better with ^{99m}Tc, because of the very short range of 2-keV electrons compared with those of the tritium β electrons of 5.7-keV average energy.

Under the most favorable condition for our optical readout device, these measurements show the very good intrinsic resolution of our gaseous detector. In these conditions, the readout surface is limited to 24 × 32 mm². Our studies show that the same resolution may be expected with a much larger surface, by using an intensified CCD camera with a larger intensifier.

Application to Biologic Samples. To validate the results obtained for the spatial resolution of the samples labeled with ^{99m}Tc, 20-μm-thick transverse rabbit kidney and brain

sections, previously injected with this tracer, were imaged and compared with the equivalent autoradiographic film (Fig. 9).

DISCUSSION

The main advantage of a gas scintillation chamber, compared with other methods for autoradiography such as photographic film and phosphor screens, is the direct recording of every particle. As with gamma cameras, these "electron cameras" are particularly suitable for quantitative measurements.

Our method of directly counting each particle emerging from the sample involves strict intrinsic linearity over a large
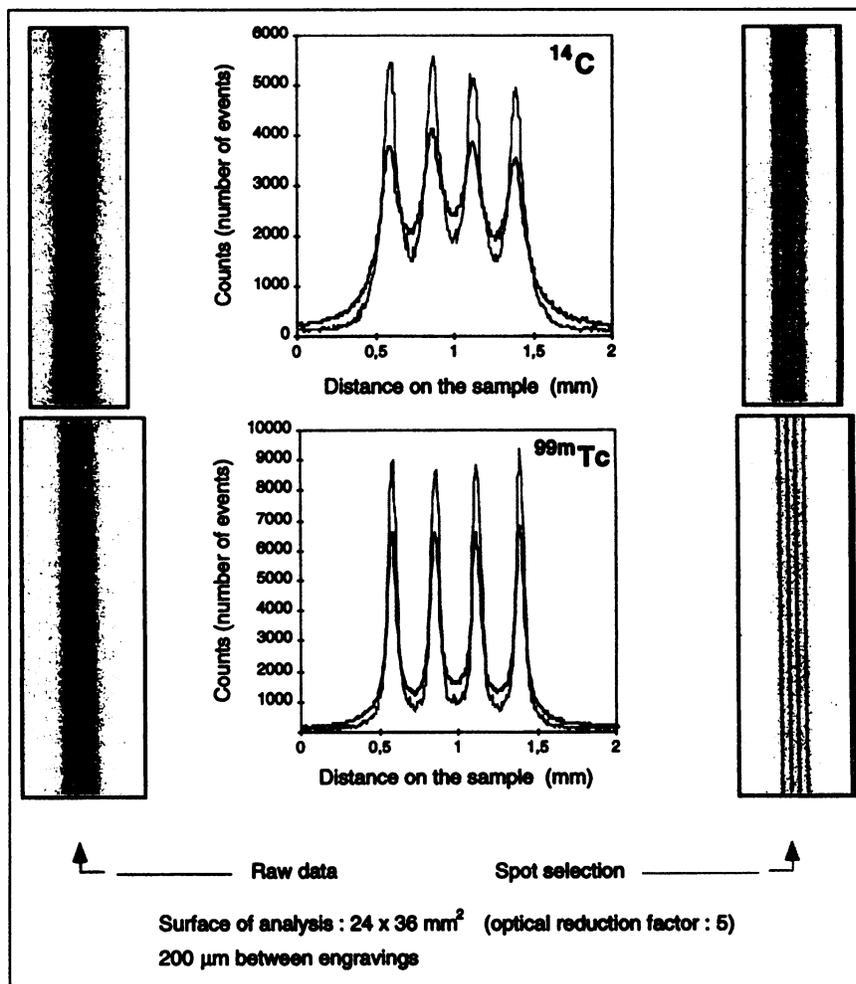
FIGURE 7. Spatial resolution measurements for ^{14}C and ^{99m}Tc. Comparison of results obtained from raw data and after spot selection.

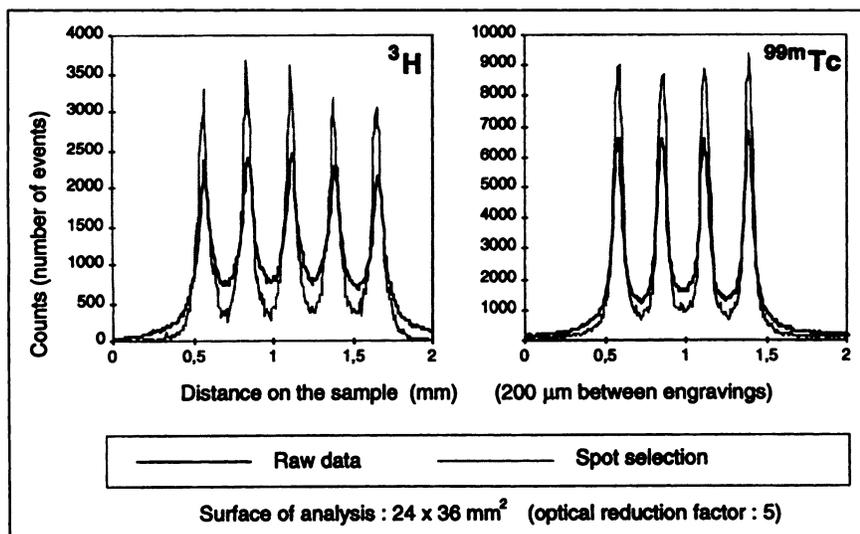Surface of analysis : 24 x 36 mm² (optical reduction factor : 5)

FIGURE 8. Spatial resolution measurements; comparison of results for ^3H and ^{99m}Tc.

dynamic range limited by noise for low activities and by saturation for the highest activities.

The first reason for saturation is the result of the readout CCD camera, which has an image rate of 50 per second. If two particles are emitted from positions very close to each other during one frame and the luminous spots become superimposed, they will be detected as only one. Therefore, the discrete limit is about 30,000 cpm/cm².

The second reason for saturation concerns the time necessary for the computer to process the data for each video frame on line. If the quantity of information in a frame is too high to be treated in 20 ms, the next frame is lost. This limit is improved about every 6 mo with improved computer technology. In any case, it has no influence on linearity for measurements during one acquisition, but only for the comparison of different acquisitions. This is because the loss of efficiency resulting from the lost frames is global, i.e., for the total image.

For high activities, then, there is a phenomenon of saturation, as with gamma cameras. However, such high activities are not usually found with common radiotracers such as ^3H, ^{14}C and ^{35}S. With ^{99m}Tc, saturation might occur.

TABLE 3
Influence of Spot Selection on Resolution Data*

Tracer		Selection limits		Resolution (µm)	Relative efficiency (%)
High amplification					
^{32}P	Raw data	$10 \leq n$	$0 \leq e \leq 1$	195	100
	Selection 1	$100 \leq n \leq 500$	$0 \leq e \leq 0,2$	150	26
	Selection 2	$100 \leq n \leq 500$	$0 \leq e \leq 0,1$	130	15
^{14}C	Raw data	$10 \leq n$	$0 \leq e \leq 1$	140	100
	Selection 1	$50 \leq n \leq 500$	$0 \leq e \leq 0,2$	130	35
	Selection 2	$50 \leq n \leq 500$	$0 \leq e \leq 0,1$	110	21
^3H	Raw data	$10 \leq n$	$0 \leq e \leq 1$	80	100
	Selection 1	$200 \leq n \leq 1000$	$0 \leq e \leq 0,2$	60	31
	Selection 2	$200 \leq n \leq 1000$	$0 \leq e \leq 0,1$	45	25
^{99m}Tc	Raw data	$10 \leq n$	$0 \leq e \leq 1$	45	100
	Selection 1	$100 \leq n \leq 500$	$0 \leq e \leq 0,2$	40	37
	Selection 2	$100 \leq n \leq 500$	$0 \leq e \leq 0,1$	30	22
Normal amplification					
^3H	Raw data	$10 \leq n$	$0 \leq e \leq 1$	100	100
	Selection 1	$200 \leq n \leq 1000$	$0 \leq e \leq 0,2$	90	50
	Selection 2	$200 \leq n \leq 1000$	$0 \leq e \leq 0,1$	80	40

*Surface analysis: 24 × 32 mm².
n = number of charge coupled device pixels in the spot; e = ellipticity of the spot (e = 1 for a circular spot and ≈0 for a long trace).
Resolution measured with different tracers in high amplification mode.
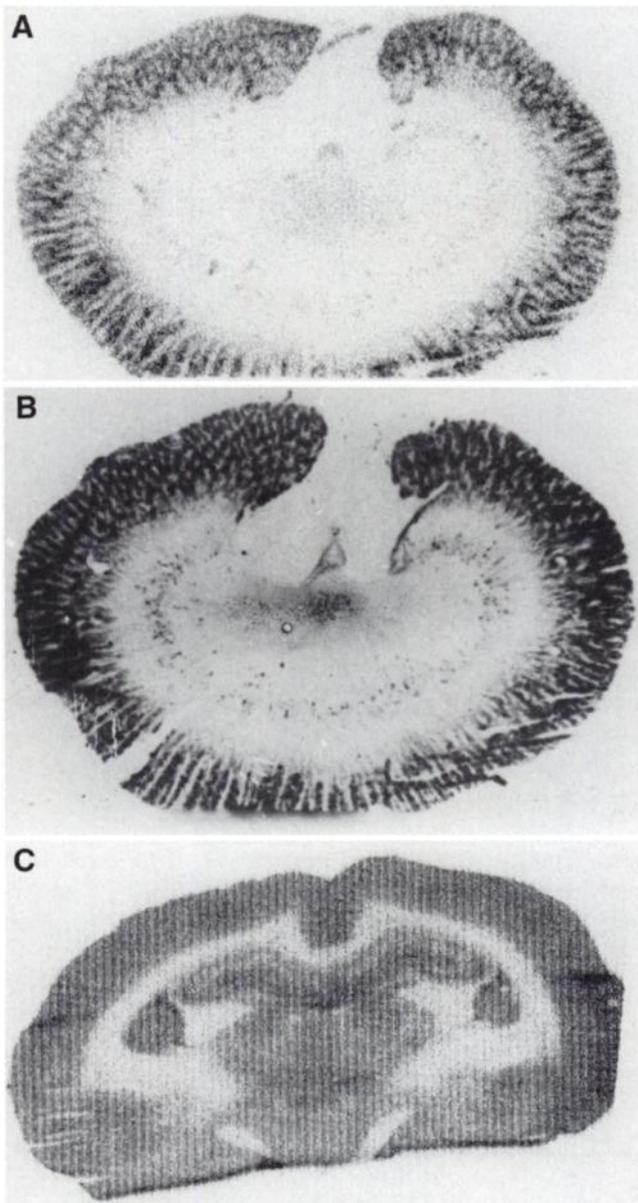
FIGURE 9. Imaging of ^{99m}Tc-labeled anatomic sections (20 μm thick). (A) Distribution of radioactivity of kidney in rabbit injected with renal tracer (DMSA) labeled with 37 MBq ^{99m}Tc 4 h before kill. (B) Spatial resolution is similar to that obtained for proximate section exposed to autoradiographic film. (C) Image of brain radioactivity in rabbit injected 30 min before kill with HMPAO labeled with 74 MBq ^{99m}Tc.

Thus, it is necessary to know the practical upper limit of the dectector's counting rate. In this way, appropriate activities can be used, thereby restricting application of the detector to its region of linearity. As long as this phenomenon of saturation is present, it will affect the complete detection system. There will be no modification of distribution of the tracer, and the comparative quantitative measurements will remain unaltered. Yet this is not so for other detectors, which can saturate at specific localized sites.

The very high sensitivity of the detector therefore is clear.

It is principally the result of the amplification of the gas chamber and the quality of the method for image reading. Virtually 100% of the particles that enter the chamber are detected, including particles of very low energy, such as the 2-keV conversion electrons of ^{99m}Tc. This sensitivity is clearly superior to that of autoradiographic photographic films, and a further advantage is that the acquisition times are of the order of 1 h. Because the complete system is very sensitive and linear over a wide dynamic range, it is well suited for the imaging of isotopes with a short lifetime.

The noise level of this detector is also very low, enabling autoradiographic studies to be performed with very small activities.

The main goal in developing this imaging system was to improve the spatial resolution of images, so as to approach that of autoradiographic films, the current reference standard. Thus, several original solutions to existing problems were found: (a) the biologic sample was placed inside the chamber; (b) use of the two-stage amplification process improved detection of electrons created near the entry point of the particle; and (c) particles were localized by calculating the centroid of the distribution of the light signal intensity. In addition, it is possible to select electrons from ^{99m}Tc with energies of either 2 or 15 keV. This is a great advantage in obtaining an image of high resolution, as shown in Figure 7.

Limits on spatial resolution are dependent on the image-reading procedure. This problem can be solved in part by reducing the dimensions of the image field. However, other technical solutions are also possible to ensure that the limits of resolution of the image reading device are less than those of the gas detector: the use of a large diameter quartz lens and improved CCD cameras with large fields (1000 × 1000 or 2000 × 2000 pixels).

The maximum spatial resolution obtained with ^{99m}Tc is of the order of 30 μm. This is slightly better than that obtained with tritium. As shown in Figures 8 and 9, the results obtained with samples of direct relevance to nuclear medicine are comparable with those obtained using conventional autoradiographic techniques.

CONCLUSION

The scintillation gas detector is an imaging device of interest to many researchers, especially those studying the radiopharmacology of molecules marked with ^{99m}Tc.

In addition, these original technological developments allow other applications to be considered. (a) Simultaneous autoradiography of two different radioisotopes, because it is possible to select β particles according to their energy. Initial studies in this direction have proved very promising. (b) Autoradiography of molecules containing positron emitters, because high detection sensitivity will prove a major advantage for the imaging of short period radioelements.

REFERENCES

1. Jacquier-Sarlin MR, Polla BS, Slosman DO. Oxido-reductive state: the major determinant for cellular retention of technetium-99m-HMPAO. *J Nucl Med.* 1996;37:1413–1416.
2. Ultee ME, Bridger GJ, Abrams MJ, et al. Tumor imaging with technetium-99m-labeled hydrazinonicotinamide-fab' conjugates. *J Nucl Med.* 1997;38:133–138.
3. Chengazi VU, Feneley MR, Ellison D, et al. Imaging prostate cancer with technetium-99m-7E11-C5.3 (CYT-351). *J Nucl Med.* 1997;38:675–682.
4. Taylor A, Hansen L, Eshima D, et al. Comparison of technetium-99m-LL-EC isomers in rats and humans. *J Nucl Med.* 1997;38:675–682.
5. Charpak G, Dominik W, Fabre JP, Santiard JC, Sauli F, Solomey N. Gaseous detectors with parallel electrodes and anode mesh planes. *Nucl Instrum Methods.* 1979;161:19–34.
6. Charpak G, Dominik W, Fabre JP, Gaudaen J, Sauli F, Suzuki M. Studies of light emission by continuously sensitive avalanche chambers. *Nucl Instrum Methods Phys Res.* 1988;A269:142–148.
7. Charpak G, Dominik W, Zaganidis N. Optical imaging of the spatial distribution of β-particles emerging from surfaces. *Proc Natl Acad Sci USA.* 1989;86:1741–1745.
8. Peskov V, Charpak G, Dominik W, Sauli F. Investigation of light emission from a parallel-plate avalanche chamber filled with noble gases and with TEA, TMAE, and H$_2$O vapours at atmospheric pressure. *Nucl Instrum Methods Phys Res.* 1989;A277:547–556.
9. Howell RW. Radiation spectra for Auger-electron emitting radionuclides: report no. 2 of AAPM Nuclear Medicine Task Group 6. *Med Phys.* 1992;19:1371–1383.